IEEE Access
Multidisciplinary | Rapid Review | Open Access Journal

Date of publication xxxx 00, 0000, date of current version xxxx 00, 0000.

Digital Object Identifier 10.1109/ACCESS.2017.Doi Number

Modeling and Simulation of Time Domain Reflectometry Signals on a Real Network for Use in Fault Classification and Location

Javier Granado Fornás[1], Elías Herrero Jaraba[2], Hans Bludszuweit[1], David Cervero[1], Andrés Llombart Estopiñan[1]

[1]CIRCE Foundation Parque Empresarial Dinamiza, Ave. Ranillas 3D, 1st Floor50018 Zaragoza (Spain)
[2] Department of Electronic Engineering and Communications, University of Zaragoza, 50018 Zaragoza, Spain

Corresponding author: Javier Granado (e-mail: jgranado@fcirce.es).

"This work was supported in by the FLEXIGRID project from the European Union's Horizon 2020 research and innovation programme under grant agreement No 864579"

ABSTRACT Today, the classification and location of faults in electrical networks continues to be a topic of great interest. Faults are a major problem mainly due to the working time spent to detect, locate and repair the cause of the fault. So, automatic fault classification and location is gaining great interest due to the cost and time savings compared to conventional location techniques. There are several state-of-the-art techniques that help to classify and locate faults. These techniques are mainly based on line-impedance measurements or in the detection of the traveling wave produced by the event caused by the fault itself. thirdly, this paper shows a technique that has given very good results based on time-domain pulse reflectometry (TDR). The physical principle is based on high frequency pulses injected into the network. These pulses are propagated through the network and returned to the injector bringing information about the state of the network. Using this technique, large distances can be monitored on a line with a single device. In addition, a real complex network and a real injector have been modeled in PSCAD^{TM} software. The combination of the TDR technique with the modeling of a real network results in high quality signals. These signals, which are very similar to the real ones, can be used for further processing by any of the existing state-of-the-art techniques, such as Neural Networks. Unlike the IEEE-13 network model, a real complex network has been modeled in this work. In addition, a real injector and a real network coupling filter have been modeled. This technique allows the verification of the model by comparing the modeled signals and the real ones obtained in the field. In addition, this work provides a database of simulated signals generated by simulation that can be used for experiments.

INDEX TERMS Fault classification, Fault location, Transmission lines, time-domain pulse reflectometry, modelling network.

I. INTRODUCTION

From a maintenance cost point of view, distribution system operators (DSOs) are specially concerned with reducing outage times. From a commercial point of view, an indeterminate number of clients lose their power supply during these periods, and some power stations (specially distributed generation, DG) may be also affected thereby. So, fault location and identification techniques are an effective method to reduce lasting outage times, considering most of the interruptions occur during a fault in the distribution network [1]–[3]. When maintenance crews are able to find the problem faster due to location techniques, the fault can be fixed earlier.

On the other hand, fault location techniques are widely used in transmission systems where each line is monitored separately. But distribution networks in real environments usually have a radial, ring or mesh topology, with many nodes and branches [4]–[8]. Therefore, location methods need a different approach to obtain a cost-effective system which can monitor the entire grid or an important section of it.

Additionally, it is also important to consider other specific characteristics of distribution systems like the presence of unbalanced loads, laterals, and different kind of cables/conductors. These features affect several assumptions of location methods, reducing their performance.

It is worth mentioning a couple of significant cases: 1) IT (Isolé-Terre) networks, which are common in distribution systems. Location is more challenging in these kind of grids [9] since classical impedance-based methods have substantial errors. And 2), Low Voltage (LV) distribution grids, which specially lack studies about fault location techniques [10]. These last networks have two important differences regarding high and medium voltage grids:

- Underground lines are commonly made up of unshielded wires
- The system end points are the customers loads, so there is a variability in their impedance value

In conclusion, on the one hand, further research is needed to find a fault location technique adapted to the special characteristics of real distribution networks, and on the other hand, more reality-based scenarios and data need to be created and shared.

Finally, the complexity of these scenarios must be accompanied by a comprehensive set of data where several electrical faults can be found. In this sense, there are several kinds of faults in power systems. For instance, series faults are produced by broken wires, and they increase the impedance of the affected lines. Or shunt faults consisting of a contact among one phase and ground and/or other phase/s. Mainly, distribution networks suffer shunt faults [11] and they, in turn, can be classified considering the number of faulty phases and the involvement of ground:

- Single line to ground.
- Double line.
- Double line to ground.
- Three phases.
- Three phase to ground.

Each kind of fault causes different electrical responses and may produce less or more hazardous effects. Thus, a complete fault-diagnosis method should be able to resolve not only the location of the faulty point but also the kind of fault found in the distribution network [12].

Our proposal, therefore, is focused on the methodology of creating real distribution networks in a simulation environment that allows us to carry out high quality and high-fidelity simulations. Not only considering the creation of different layouts, but also having the possibility to simulate with different types of faults.

Additionally, and based on the above, the contribution of the present paper is built over the next points:

1) To demonstrate the methodology to model a real distribution network, the injector device, and the coupling device.
2) To demonstrate that we can simulate the pre-fault and fault state of the network and obtain the network response signals.
3) To demonstrate that the signals obtained are of sufficient quality to be used in post-processing to detect or locate faults.
4) To provide a database of 200 signals simulated from a real network to serve as a tool for future studies

II. ENVIRONMENT

Today, electrification has become one of the paradigms of our society. The technological progress that humanity is undergoing generates an unprecedented dependence on electricity.

In this context, distribution networks play a fundamental role since a service failure can have catastrophic consequences. Examples include the dependence of telecommunications, aviation, the medical industry (which is becoming more and more technologically advanced), the arms industry and, of course, the dependence of today's society on artificial lighting.

It is essential that transmission and distribution infrastructures (as well as distributed generation) are robust to any circumstance that could leave grid users without service. So, the classification and location of faults in power grids [13], has become an essential objective to achieve the objective to reduce non-productive times. But even today, the task of localization, specially, in distribution networks is still a difficult task that involves the displacement of specialized personnel with ground or aerial means throughout the affected section. All this has led to make an effort to advance in the automatic location of faults. The central idea in automatic fault location is to detect the fault and its type, as well as to locate the distance to the fault as accurately and quickly as possible.

Nowadays, to repair a fault, the section where it has occurred must be checked and the exact point must be found by visual inspection. The immediate objective of automatic fault location is to be able to tell maintenance personnel the exact location of the fault so that they do not have to search for it.

As a future goal, automatic fault localization will allow the development of the network self-repair paradigm. In this case, the networks themselves will automatically disconnect only the affected section, isolating a minimum segment of the network (where the fault occurred). The rest of the section is supplied by another redundant path. For this to be possible, the networks must be highly meshed, i.e., have a radial and highly redundant topology.

This tendency of networks to be highly meshed makes it even more difficult to locate faults in a given section.

In addition to the need for fault location, fault detection and classification may also be necessary. In some lines (transmission lines and some distribution lines), there are fault passage detectors [12]. These systems monitor the voltage and current of the network. When a fault occurs, the device detects it and can alert a second system to locate the fault.

However, usually in low voltage lines, these last systems are not available due to their high cost, so the detection and classification of faults is a necessary preliminary step for the subsequent fault location.

In this paper, we address the task of modelling a real complex distribution network in order to, subsequently, by means of simulation, be able to generate network response signals to the pulses injected into the network.

This response is produced not only with the network in pre fault state but also with the network once a fault has occurred (also simulated). With these data, a representative database is obtained to be processed later with different fault location algorithms.

As already mentioned, the physical principle used to obtain these signals is time domain reflectometry (TDR) [14], [15]. The injected signal propagates through the network and bounces (at each impedance change) and returns to the locator bringing information about the state of the network.

It basically consists of performing periodic injections of pulses into the line in each of the phases of the network (R-S-T) so that the electrical response of the network is updated frequently. When a fault occurs, the response signal is different from the signal received when the network was operating normally.

This reflection of the pulses makes it possible to record at the injection point all the signals that "come back" after "bouncing" through the different bifurcations of the network. These signals are digitized in the injector itself and then processed by an algorithm to locate the fault.

III. STATE OF THE ART

The structure of the state of the art is shown below. First, a change of scenario from IEEE 13 simulations to a real network is shown. Then we will discuss the modelling of the Injector and the filter and at the end a review of the main localization and classification techniques is given.

A. Change of scenario: from IEEE-13 to real network modeling.

The IEEE 13 bus feeder is a small system that is used to test distribution systems. It operates at 4.16kV, has 1 source, a re gulator, a number of short unbalanced transmission lines, and shunt capacitors. Fig. 1 shows the one line diagram of the test system .

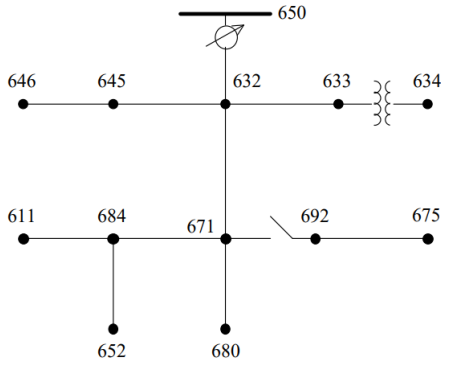

FIGURE 1. One-Line Diagram of IEEE 13 Bus Power System .

There are multiple publications using the IEEE 13 network to develop fault location or classification algorithms [16]–[19] This networks may be suitable for making comparisons of different techniques or algorithms, but since it is a simulated network that has no correspondence with a real network, the simulations cannot be verified.

In our work, we have modeled a real network containing 25 nodes. This network has been modeled with the real data of cable models and node impedances.

It has been possible to verify that the signals obtained by the simulator correlate with the signals recorded in the field. These signals can be used to develop reliable fault classification and location algorithms.

Using a model of a real network, the aim is to take a further step towards the development of fault detection and localization algorithms.

B. Modeling of Injectors and Couplers

By modelling the signal injector and the grid coupling filter, together with the modelling of the grid itself, we are able to perform simulations fairly close to reality and thus develop more accurate algorithms that can be validated in the field.
In the TDR technique, high frequency pulses are injected into the network. In order to inject the pulses and receive the response from the network, we uses an injector and a coupler devices [20].

The injector is basically a voltage source whose output can be switched for a certain time in order to obtain the required pulse width.

Between the injector and the network, the coupler is placed. The coupler is basically a filter that lets the high frequency pulses through in one direction and blocks the low frequency (50 Hz) of the mains in the other direction [21], [22].

In this work we have modelled the injector and the real coupler used in the prototype installed in the field.

C. Localization and classification techniques

Multiple techniques have been proposed to address the fault location problem. However, all methods can be grouped in three main categories: impedance measurement, travelling waves and artificial intelligent.

1) IMPEDANCE MEASUREMENT

This methodology consists in measuring the apparent impedance at the rated frequency from a single point within the electrical network. The impedance measurement changes between a healthy and a faulty line. Moreover, the impedance variation is related to the fault distance. So, if the apparent impedance is being monitored during a fault occurrence, it is possible to determine the failure location.

The main advantage of this method is to work with steady state values. Thus, the required acquisition device can be relatively cheap and simple. Nevertheless, distribution networks have inherent characteristics which introduce substantial errors to this technique [23]–[25]:

- Non-uniformity of the lines
- High impedance faults specially in IT grids
- Radial topology leading to the multi-point location problem
- Unbalanced loads among phases

Furthermore, the presence of distributed generation becomes impedance-based methods more challenging [26]. Accordingly, this methodology does not seem the most suitable solution for location in the new paradigm of power distribution networks.

2) TRAVELLING WAVES

Well-known propagation of electromagnetic waves through transmission lines is the basis of this location method. Mainly, telegraph equations describe this phenomenon where two important properties allow locating faults in power systems:

- Waves travel with a certain speed depending on the wire properties.
- Any impedance change along the line produces a partial reflection of the electromagnetic waves.

There are two main approaches to this technique:

- Measuring the transient signal produced by the fault. This approach is widely used in transmission systems [27] where lines are monitored separately. However, in distribution networks, those transient waves experience multiple reflections due to the topology. Therefore, the signal intensity may be too much low when it arrives to the locator, making difficult locating the origin of the fault. Many alternatives have been proposed to fix this challenge [11], [25], [28]–[33]. On the one hand, some of them require the installation of many complex and synchronised devices, thus the solution is not cost-effective. On the other hand, the single-device approaches rely on either complex mathematical transformation or grid simulations. Both solutions require offline calculation, and the latter is model dependent.
- Injecting a high frequency signal and measuring the reflected wavefronts. This technique is commonly named as TDR. However, distribution networks have many forks where the travelling wave is reflected, hence the electrical response of the grid is complex. Several solutions [30]–[32] have been proposed to overcome this problem, but all of them require difficult boundary conditions or have not proved to solve the problem in a real network yet.

Summarising, TDR have demonstrated good results in distribution systems, both in Medium Voltage (MV) and LV networks [33], but further research is needed in order to obtain a generalised and cost-effective method.

3) ARTIFICIAL INTELLIGENT

There are several approaches within this discipline. Regarding fuzzy logic, it is still not clear the number of necessary fuzzy functions to define the problem. Genetic algorithms introduce unacceptable uncertainties considering this application. Whereas support vector machines and artificial neural networks seem to fit for fault location. Thus, many works can be found about applying these two methods to locate faults in distribution networks, usually combined with other techniques [34], [35].

However, these approaches always find the same problem: it is really difficult to achieve an adequate database to train the algorithms due to the needed amount of data and a lack of measured waveforms from faulty lines. Therefore, nowadays each training is based on simulations and every proposed method strongly relies upon the grid model, requiring a re-training when any characteristic of the electrical grid changes [10], [36][1. Additionally, further investigations are needed in order to increase the accuracy of these methods in fault location [35].

IV. THEORY

A. Telegrapher's equations

For the study of transmission lines, the model used consists of a temporal discretization of the lines, i.e., an infinitesimal analysis of the line is performed to understand the temporal and spatial evolution of both voltage and current.

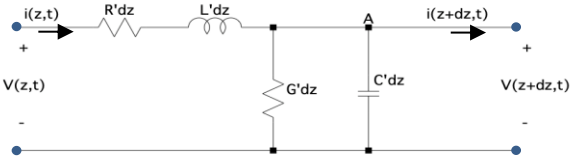

FIGURE 2. Infinitesimal portion of a transmission line.

For this purpose, the line is modelled as shown in Fig. 2, and the differential equations obtained are called the telegrapher's equations (the complete process of this model can be studied in []).

$$\frac{\partial i(z,t)}{\partial z} + G' \cdot v(z,t) + C' \cdot \frac{\partial v(z,t)}{\partial t} = 0 \quad (1)$$

$$\frac{\partial v(z,t)}{\partial z} + R' \cdot i(z,t) + L' \cdot \frac{\partial i(z,t)}{\partial t} = 0 \quad (2)$$

In these equations, as can be seen, both the temporal and spatial evolution are mathematically defined. Therefore, from them it is possible to extract the information of how an electrical signal behaves in an electrical conductor.

The most general solution to the above equations for voltage and current is:

$$v(z,t) = V^+ \cdot e^{(jwt-\gamma z)} + V^- \cdot e^{(jwt+\gamma z)} \quad (3)$$

$$i(z,t) = I^+ \cdot e^{(jwt-\gamma z)} + I^- \cdot e^{(jwt+\gamma z)} \quad (4)$$

where V^+, V^-, I^+ and I^- represent the amplitudes of the corresponding waves.

By decomposing into two independent signals labelled with superscripts + and -, respectively:

$$v^+ = V^+ \cdot e^{(jwt-\gamma z)} \quad (5)$$
$$i^+ = I^+ \cdot e^{(jwt-\gamma z)} \quad (6)$$

Corresponding to the voltage and current wave propagating in the direction of increasing z, i.e. in the direction from the generator to the load. These are called progressive waves.

Similarly, we refer to waves propagating in the direction of decreasing z, or from the load to the generator, in the following equations:

$$v^- = V^- \cdot e^{(jwt+\gamma z)} \quad (7)$$

$$i^- = I^- \cdot e^{(jwt+\gamma z)} \quad (8)$$

which we will call regressive waves. These regressive waves are generated when the progressive wave is reflected in the load.

Equations (3) and (4) show that at any point on the transmission line, z, and at any instant, t, the measured voltage, and current are the sum of the values of the two corresponding waves (progressive and regressive).

Thus, all the points on the transmission line experience the same variation as a function of time, the factor $j\omega t$, but with a delay due to the position, the factor γz, which will be greater the greater the greater the distance from the origin on the z-axis.

B. Morphology and configuration of injected signals

Taking advantage of the behavior explained in the previous section, in which the nature of the emission of a signal on a transmission line produces a return signal, we can use the latter as a "tracking" signal in search of possible disturbances in the distribution network.

In this way, electrical pulses (24 V) will be injected into the network itself, which will give us updated information on the status of the network. In other words, a pulse sent to the grid in its normal state will return a series of very different return signals to those that would be received when the pulse is sent when the grid is at fault.

The state of the distribution network prior to the time of the fault (with the network in its normal state) will be called the *pre-fault state*. And consequently, the state of the network once the fault has occurred, we will call it the *fault state*.

In other works, such as [35].it is proposed to inject pulses into the grid at zero crossings of the grid voltage waveform. Therefore, this imposes important restrictions on the number of pulses to be injected, mainly because the time available to inject the pulses is limited to the interval between the detection of the fault and the subsequent opening of the line breaker.

In our approach we suppress the dependence of the injection on zero crossings and allow them to be generated at any time.

The parameters used in the implementation proposed in this article are the following:

Sampling frequency: The proposed three-phase prototype, having no limitation on the number of pulses to be injected, reconstructs the system response from the injection of four pulses, which allows obtaining a reconstructed signal with a frequency of 100 MHz

Injected pulse width: There is a blind zone, defined as the distance below which the proposed system is unable to locate any faults accurately. During this period of time the system is unable to detect any disturbances or changes occurring in the power grid, which corresponds to the blind zone of the system. Therefore, to reduce the blind zone, the width of the injected pulse has been reduced to 10 ns.

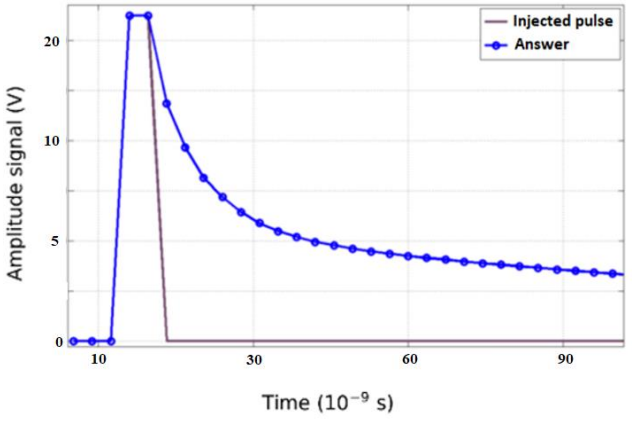

FIGURE 3. Pulse width 10 ns and response to that pulse (sampling frequency 100 MHz)

Fig. 3 shows a pulse width of 10 ns, sampled at a frequency of 100 MHz It shows how the system response diverges at sample n=2 (taking n=0 as the instant where the pulse starts). The blind zone is calculated from the sampling frequency of the equipment (fs) and the propagation velocity of the pulse on the line (v) according to:

$$d = n \cdot \frac{v}{2 \cdot f_s} \quad (9)$$

where n is the sample number where the response diverges.

Thus, considering a pulse propagation velocity of $1{,}65 \cdot 10^8$ m/s, and at the sampling frequency of 100 MHz, the blind zone for such a pulse is 1,65 m. However, for a pulse width of 2.5 ns, and taking the same sampling frequency and propagation speed, the first variation in the response will be seen in sample n=5, which is equivalent to 4,125 m of blind zone.

Equipment input impedance: An important addition that has been considered in our approach is the modification of the input impedance of the system. This prevents the reflected pulse from being reflected to the system connection point. Also, to achieve a greater range when detecting or locating faults, a high impedance has been set at the input of the system.

C. Network response to injected signals

At the moment when the waveform appears, a voltage originates at the power line input, the propagation of which continues until a point of discontinuity is reached, where a change of characteristic impedance occurs, as shown in Fig. 4.

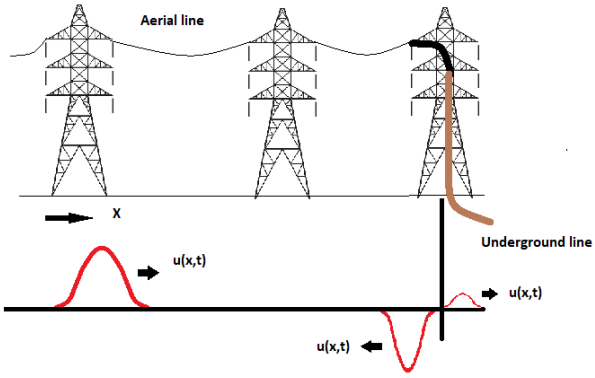

FIGURE 4. Incident, reflected, and transmitted waves at a discontinuity due to a change in impedance.

Through the characteristic impedance line Z_{0L} of the diagram in Fig. 3 an incident voltage wave u^+, and hence a current wave given by:

$$i^+(x,t) = \frac{u^+(x,t)}{Z_{0L}} \quad (10)$$

When u^+ reaches the point of discontinuity, a reflected wave u^- originates and propagates to the left, superimposing itself on the incident wave. Also, part of the incident wave is transmitted into the new medium, giving rise to a wave u^t. For the continuity of the electric potential is complied with:

$$u^+(x,t) + u^-(x,t) = u^t(x,t) \quad (11)$$

Similarly, the continuity condition for the current is fulfilled at the point of discontinuity:

$$i^+(x,t) + i^-(x,t) = i^t(x,t) \quad (12)$$

Therefore:

$$\frac{u^+(x,t)}{Z_{0L}} - \frac{u^-(x,t)}{Z_{0L}} = \frac{u^t(x,t)}{Z_{0C}} \quad (13)$$

We can therefore define the reflection coefficient at the point of discontinuity as:

$$\zeta = \frac{u^-(x,t)}{u^+(x,t)} = \frac{Z_{0C} - Z_{0L}}{Z_{0C} + Z_{0L}} \quad (14)$$

In a zero-loss power line, these characteristic impedances do not depend on the frequency, and therefore, after transformation to the frequency domain, the reflection coefficient remains the same.

On the other hand, it follows from () that when the impedances of both power lines are equal, $\zeta = 0$, i.e., there is no reflected wave, and the lines are said to be matched. In the case of a short-circuit in the line, the impedance Z0C can be considered as 0, so $\zeta = -1$, or in other words, $u^-(x,t) = -u^+(x,t)$, i.e. at the point where the short-circuit has occurred the entire incident wave is reflected. In the same way it follows that, in the case of an open line ($Z_{0C} = \infty$), the reflection coefficient is equal to unity, the transmitted wave being twice the incident wave.

To derive equation (14), the load impedance or characteristic impedance Z_{0C} has been considered purely resistive. However, when this impedance is reactive, the reflection coefficient in the time domain becomes a function of time and, therefore, the reflected wave $u^-(x, t)$ is defined as the convolution product between the incident wave $u^+(x, t)$ and the reflection coefficient $\zeta(x,t)$:

$$u^-(x,t) = u^+(x,t) * \zeta(x,t) \quad (15)$$

Finally, another parameter to consider would be the transmission coefficient τ, which would be defined as the ratio between the transmitted and the reflected waves:

$$\tau = \frac{u^t(x,t)}{u^+(x,t)} = \frac{2 \cdot Z_{0C}}{Z_{0C} + Z_{0L}} \quad (16)$$

Whose relationship with the reflection coefficient would be:

$$\tau = 1 + \zeta \quad (17)$$

V. METHODOLOGY

This section describes the methodology to obtain response signals from an electrical network using the TDR technique. We will start by explaining our proposed system from the basic building elements (which need to be modelled accordingly), continue with the modelling of the electrical network itself, and finally, the relevant simulation process will be explained. Therefore, the following three sections will be explained in detail:

- Blocks Modeling
- Network Modeling
- Simulation Process

FIGURE 5. Methodology block diagram

VI. BLOCKS MODELING

This section describes the basic blocks modelled. It contains a generic grid connection, cables, loads, filters, and the pulse injector.

A. Grid connection model

The system includes the CT (transformer), but also the MV connection, modeled with an ideal source and an R-L impedance that reflects both the Scc and the R/X ratio of the network upstream of the transformer.

The Scc is the short-circuit power of the upstream MV network without the CT, from which the LV model hangs and where the pulses are injected.

The grid connection of the LV network has been modelled with an adjustable RL-based equivalent load together with a transformer, as shown in Fig. 6.

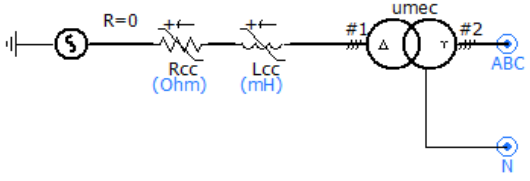

FIGURE 6. change in impedance.

Parameters of the model are:

- Short circuit power (MVA): 20
- X/R ratio: 10
- High voltage (kV): 15
- Low voltage (kV): 0.4
- Transformer power (MVA): 0.5

The RL equivalent parameters Rcc and Lcc are calculated from the short circuit power and X/R ratio.

Several tests have been carried out to evaluate the impact of a variation of the R-L equivalent of the upstream MV network. The system response was tested for values of Scc = 5, 10 and 20 MVA and X/R = 10, 5 and 1. For all combinations, almost identical results were observed. Only the nominal power of the LV transformer has been found to be relevant only for the short-circuit transient, which is attenuated less with a 50 kVA transformer, than with 500 kVA. Therefore, typical values have been chosen for the experiment setup.

B. Load models

Loads are very critical in a LV network configuration, as they behave similar to faults. Load variations will cause different reflection pattern, which means, that the obtained reflected signal will be very noisy. In this sense, four different load models have been implemented:

- No load (1 GΩ).
- Single-phase load.
- 3-phase symmetric load.
- 3-phase asymmetric load (several single-phase loads at the same bus).

The loads in the model have been derived from historical smart meter data of active and reactive power. Average values have been converted into R and L, assuming nominal voltage. 3-phase meters were implemented as symmetric 3-phase loads. Single-phase meters are modeled as such, but in occasions, several clients are connected to the same bus. In this case, all loads are aggregated and modeled as an unbalanced 3-phase load.

C. Cable models

The grid model contains detailed models of the cables, including 5 different types. In LV networks, cables are not shielded, which means that HF signals travel partly outside the insulator and may have some interference with neighboring conductors. This is a fundamental difference compared with medium voltage (MV) networks, where cables are typically shielded. Geometrical cable parameters are:

- Number of conductors
- Conductor radius
- Insulator radius (measured from conductor center)
- Conductor distance from ground
- Conductor distance relative to each other
- Cable type: aerial or underground

All cables are considered to have 4 conductors, where the neutral wire may have a different diameter.

Apart from the geometric parameters, the frequency dependent model has another set of parameters. The adopted values shown in Table have been adjusted during model testing. The fitting accuracy needed to be increased compared to the default values, in order to avoid numerical oscillations.

Namely, starting frequency was reduced from 0.5 Hz to 0.1 Hz and end frequency increased from 1 MHz to 1 GHz. Frequency increments where increased from 100 to 500 and fitting errors were reduced from 0.2% to 0.1%. Finally, DC correction was modified from "Disabled" to "Functional Form".

TABLE I
OPTIONS OF THE FREQUENCY DEPENDENT CABLE MODEL.

Model option	Value
Travel Time Interpolation	On
Curve Fitting Starting Frequency	0.1 Hz
Curve Fitting End Frequency	1 GHz
Total Number of Frequency increments	500
Maximum Order of Fitting for Yc	20
Maximum Fitting Error for Yc	0.1 %
Max. Order per Delay Grp. for Prop. Func.	20
Maximum Fitting Error for Prop. Func.	0.1 %
DC correction	Functional Form
Passivity Checking	Disabled

D. Pulse injector device model

The injector device mainly consists of a HF pulse generator and data acquisition with very high time resolution, which permits registration of oscillations in the ns-range. The pulse is created by a switch and triggered by a pulse controller. Pulse amplitude was fixed at 24 V.

Within the simulation, this controller generates one trigger before the fault event, creating the reference response and another one after the fault event. It may be mentioned here that one trigger event consists of 3 triggers (one for each phase), with a time delay of 0.5 ms between them. This time delay is necessary, in order to get the necessary attenuation of the pulse response, because oscillations are induced in all 3 phases.

For the pulse generator, two different options were implemented, in order to study the differences in the response. One option was a sinusoidal signal of one period and the other one was a rectangular pulse of half-period duration. With 1 MHz pulse frequency, this means for the pulse a duration of 500 ns.

Simulation tests revealed that an ideal rectangular pulse was not suitable. Due to the detailed time-domain model, infinite ramps create singularities and the model did not converge. Therefore, a more realistic pulse was implemented where the switch is modelled as a controllable resistance with a defined "on" resistance (R_{on} fixed at 10 mΩ) and "off" resistance R_{off}. A ramp rate defines how fast the transition between R_{on} and R_{off} will occur. In the model (Fig. 7), this realistic switch model received two parameters:

- R_{off}: 1 MΩ ("off" resistance of the switch)
- ramp rate (200 ns from low to high)

These two parameters have been adjusted together with the network filter (see next section), in order to minimize oscillations induced by the switch.

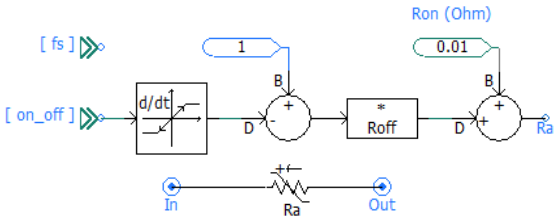

FIGURE 7. Realistic switch model with controlled switch ramps

E. Coupler device model

The injector device is connected to the network through a filter called "Coupler" which aims to remove the grid frequency (50 or 60 Hz) and harmonics. A simple high-pass L-C filter has been used for this purpose in the model (Fig. 8). The desired design frequency of 100 kHz can be obtained by many possible combinations of L and C. Tests have shown that many combinations, especially with a large capacitance cause oscillations when the 1-MHz pulse signals are injected.

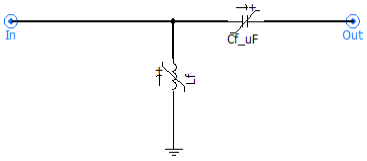

FIGURE 8. Realistic L-C network filter.

Oscillations could be reduced to an acceptable level designing the high-pass filter with L-C values of 25.3 µH and 100 nF respectively. Note that these values are only valid together with the ramp parameters of the switch. Therefore, in a real device, filter design will be very critical. The Fig. 9 shows the Bode plot response diagram of the filter.

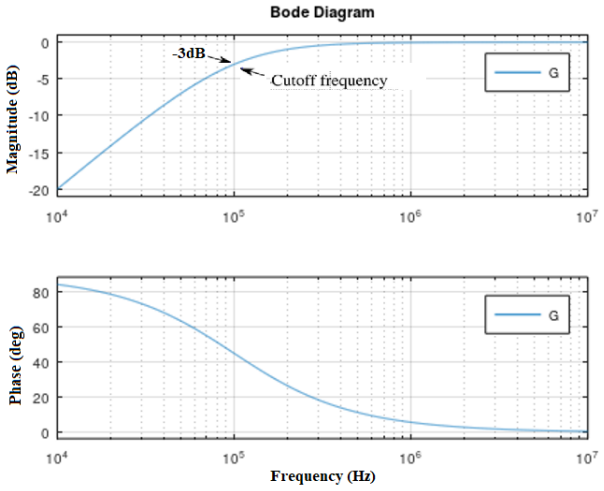

FIGURE 9. Filter Bode plot response diagram

VII. NETWORK MODELING

Next, this section describes the network modelled. It contains the relations between the basic blocks of the previous section. A diagram of the real network modeled is shown in Fig. 10.

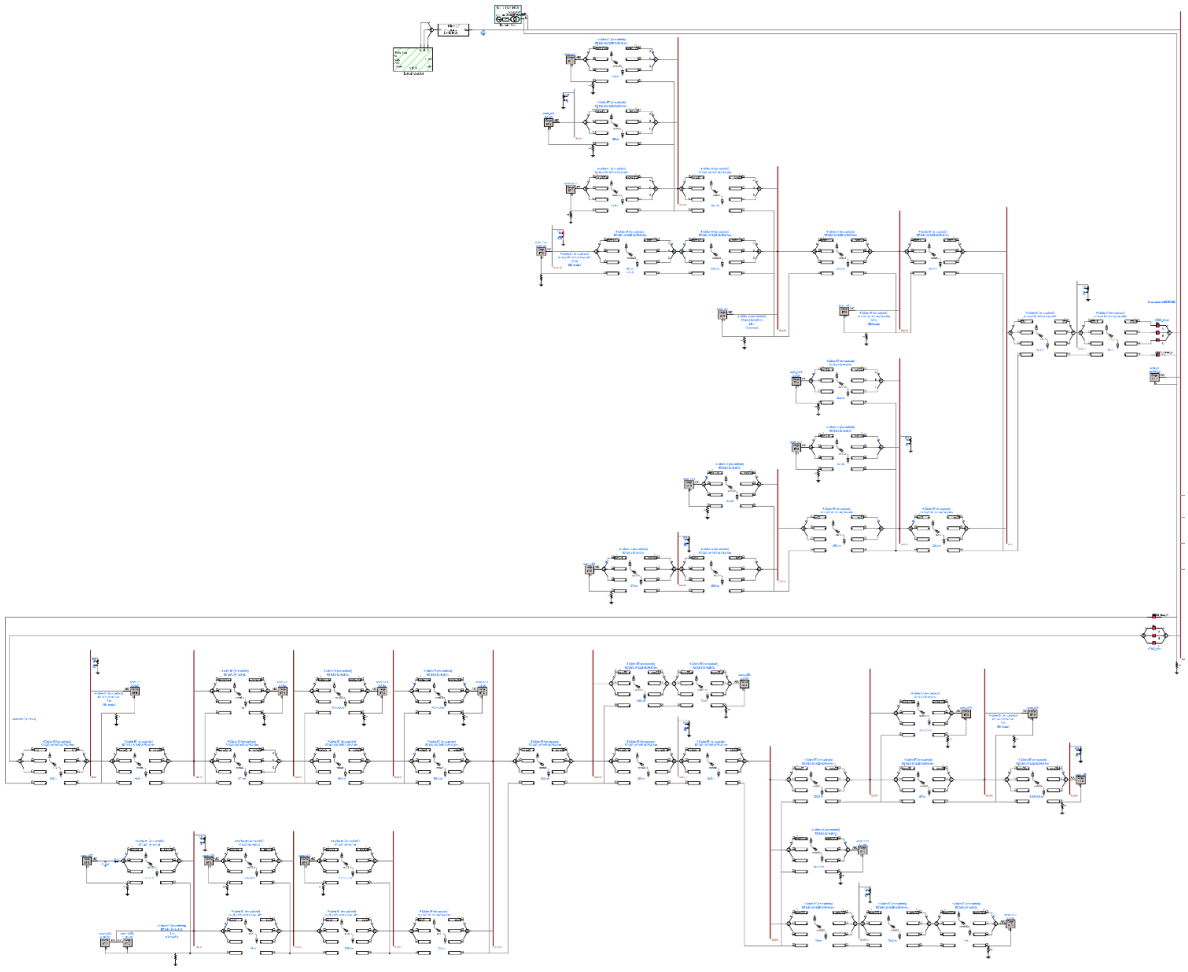

FIGURE 10. Diagram of the modeled real network

The diagram shows the following elements:

A. ***Fault Locator (Fig. 11):*** This is the element that injects the pulses and subsequently digitizes the network response signals. These signals return after bouncing in all impedance changes (loads, bifurcations, cable type changes, faults, etc...).

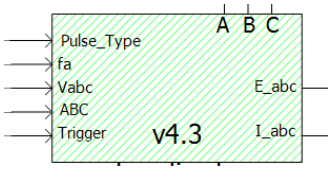

FIGURE 11. Fault Locator

Inside this block (Fig. 12), you can see the pulse injector circuit for phase A, with continuous source Va (pulse), phase selection (switch A). The signal "pulse A" triggers the injection and comes from the "trigger" input.

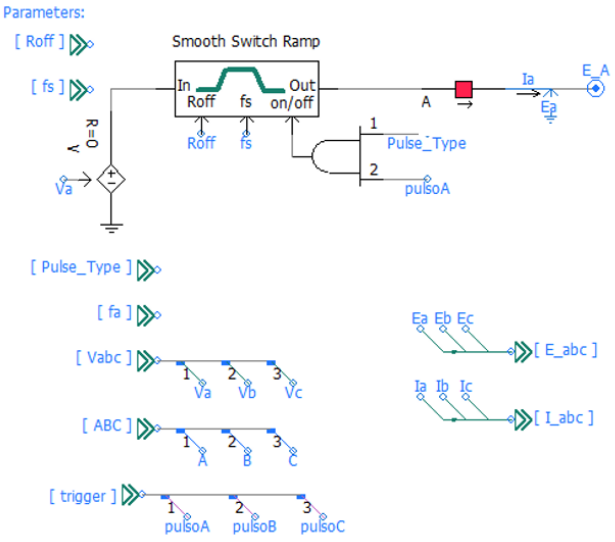

FIGURE 12. Inner Fault Locator

The Fig. 7 shows the inner of the Smooth Switch Ramp block.

PSCAD models the electronics (transistors, IGBTs, etc.) as ideal switches (no ramping). It has been observed that this introduces extreme transients in the model, especially when a pulse is injected. The mains LC filter has been identified as the cause, which has some sensitivity to high dU/dt ramps. By adjusting the L and C values of this filter, the effect can be minimized, but not eliminated.

To solve this problem, a new module called "Smooth Switch" has been created as an element to connect and disconnect the source to inject the pulse. This element is intended to create a more realistic pulse with controlled edges to avoid extreme ramps.

D. L-C Network Filter (Fig. 13): This is the element that is placed between the injector and the mains as an insulator against the mains voltage. It is a filter for the mains frequency (50 Hz) but allows high frequency pulses to pass in both directions.

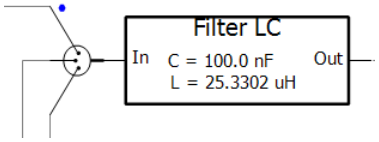

FIGURE 13. L-C Network Filter

E. Detail of network section (Fig. 14): The bifurcation, the distance of the section, the type of cable used and the type of load at the end of the section are shown.

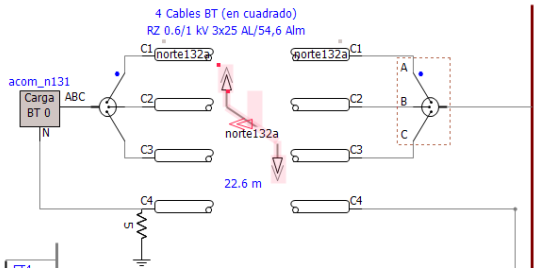

FIGURE 14. Detail of network section

F. Definition of fault: The faults can be placed at any point in the network. Their impedance value and type can also be defined. Fig. 15 shows a fault (FT1), placed in the middle of a cable run and Fig. 16 shows a fault (FT4), placed at the end of the run before the load.

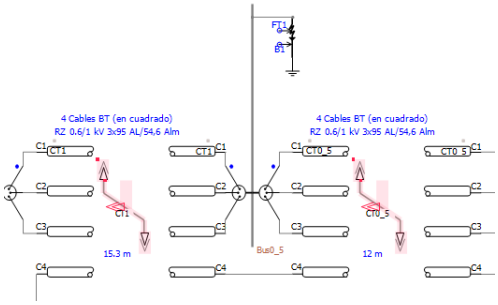

FIGURE 15. Fault FT1 in the middle of a cable run

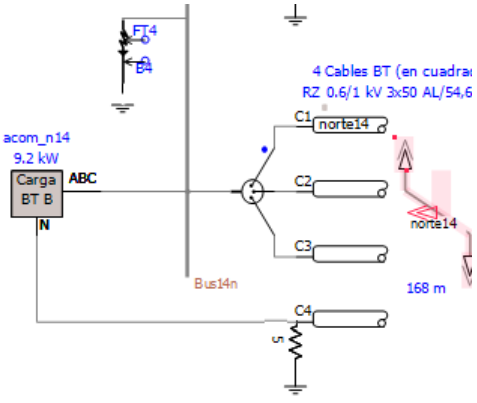

FIGURE 16. FT4 failure at end of run and before the load

VIII. SIMULATION PROCESS

A. Simulation Parameters

This section explains all the parameters that can be set when performing a fault simulation.

Types of faults: Up to 10 different fault types can be defined in the simulation (Fig.17):

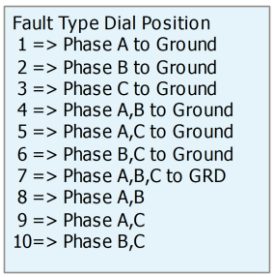

FIGURE 17. Combinations of fault types

Position of the fault: The faults can be placed at any point in the network. In our case we have placed 10 faults at different distances from the injector (Fig. 18):

Number of Fault	Name of bus	Distance from TDR (m)
1 (FT1, B1)	Bus0_5	12
2 (FT2, B2)	Bus2	40
3 (FT3, B3)	Bus11s	283
4 (FT4, B4)	Bus14n	933
5 (FT5, B5)	Bus13s	757
6 (FT6, B6)	Bus29n	1833
7 (FT7, B7)	Bus261n	1274
8 (FT8, B8)	Bus23s	594
9 (FT9, B9)	Bus25_5n	968
10 (FT10, B10)	Bus122n	520

FIGURE 18. Localization of faults in the network

Impedance of the fault: Different types of impedance can be associated to each of the defined faults. In our case, we have defined four impedance values (Fig. 19), ranging from a very low impedance fault or short circuit (0.01Ω) to a high impedance fault (1000 Ω) :

1	0.01 Ω
2	80 Ω
3	150 Ω
4	1000 Ω

FIGURE 19. Fault impedance values

Load values: Each of the network loads can be modeled as a resistance plus an inductance. In our case, since it is a real network, the actual data of the existing loads have been used (Fig. 20).

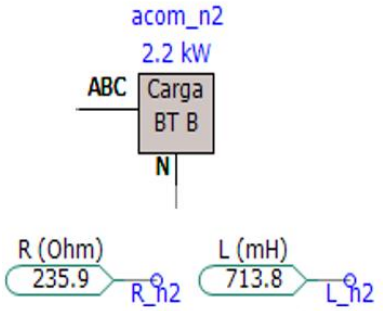

FIGURE 20. R and L are values of load n2

Injected pulse values: The injected pulse can be parameterized by varying its width, amplitude and time delay between phases (Fig. 21).

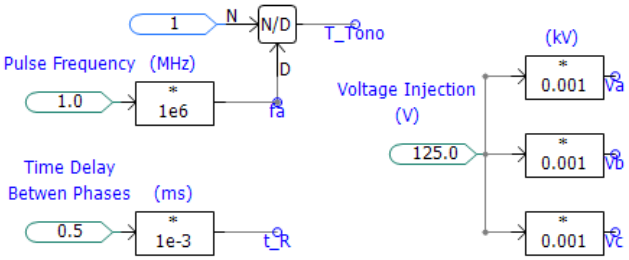

FIGURE 21. Voltage (V) and pulse rate (MHz)

Injection time values: The pulses can be parameterized to be injected at the most convenient time in each case. The fault event time can also be fixed(Fig. 22).

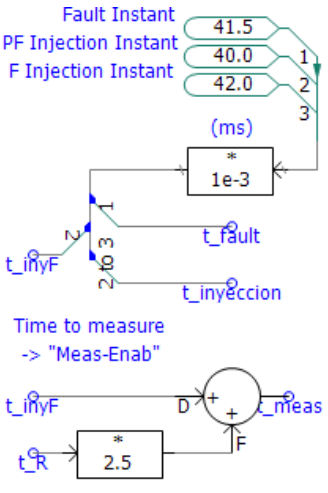

FIGURE 22. Injection time parameters

Miscellaneous simulation time considerations: The simulation process starts with a waiting time of about 0.04s to reach the steady state. This process is necessary because the simulator starts the process by abruptly imposing the defined voltage on the line.

Once the steady state has been reached, a pulse is injected in each phase (R-S-T) at defined width and amplitude. Pulses injected in one phase can be induced in adjacent phases. To avoid this problem, it is necessary to wait until the pulse in one phase is extinguished before injecting in the next phase. This time depends on several factors such as pulse voltage, pulse width and the line response itself. This value is adjusted by trial-and-error with only one simulation case before launching all final simulations.

The simulation of each case needs about 160 s of execution time (running in intel core i7 7th gen). This time is for the specific case of the real network simulated in this work. The more complex the network, the more runtime each simulation needs.

The total number of simulated faults and the total time required for the simulation can be calculated as follows:

- Having 14 fault locations in the network. These locations have been chosen to have a wide range of distances to the injector and at various bifurcations.
- with 10 different types of faults.
- and 6 possible types of injection that arise from the combination of the number of phases in which we inject: Inject in all three phases, two by two or one by one.
- and finally, a range of fault impedances from 0.01Ω to 1000Ω. Making 5Ω steps, we have 200 values for each fault.

According to (1), with all these data, if we wanted to simulate all the combinations, we would have:

$$\frac{14\ (nodes) \times 10\ (fault\ types) \times 200\ (impedance\ values) \times 6\ (Injection\ types) \times 160s}{3,600s\ \times 24h} = \frac{168,000\ (examples) \times 160s}{3,600s \times 24h} = 311\ days \qquad (18)$$

The complete simulation to obtain 168,000 examples would cost almost a year. It is a major problem with respect to simulating a real network. This is especially true for those classification or localization techniques based on neural networks because these types of techniques require a large number of examples for training. In [37]

B. Results of simulation runs

With the model set up and all design values adjusted, a multi-run simulation plan was developed to create a number of different scenarios that can be feasibly simulated in a reasonable amount of time.

Bearing in mind that it must be possible to repeat the simulation in order to modify any of the parameters, we decided to select:

- 10 different fault locations within the network, covering cases of faults at different distances
- 4 fault resistances: 0.01, 80, 150 and 1000 Ω
- 5 fault types:
  - Phase-to-ground (R)
  - Phase-to-ground (S)
  - Phase-to-ground (S)
  - Between 2 phases (R-S)
  - 3-phase-to-ground

All combinations were simulated, obtaining a total of 200 results.

Considering that each simulation costs about 160s, the 200 simulations take about 9 hours. This gives us a reasonable margin to run different simulations until we get the one that best suits our needs.

The simulation time step was 10 ns and results were saved at a sample rate of 50 ns. Before starting the multiple run, the pre-fault references are obtained from a separate simulation. A snapshot (data acquisition) with a duration of 1.51 ms is saved after 40 ms, when stationary conditions are reached. One reference response is obtained for each pulse type (pulse or sinusoidal). In Fig. 23 the three responses in voltage can be observed, showing that the responses are completely attenuated after 0.5 ms, before the next pulse injection starts.

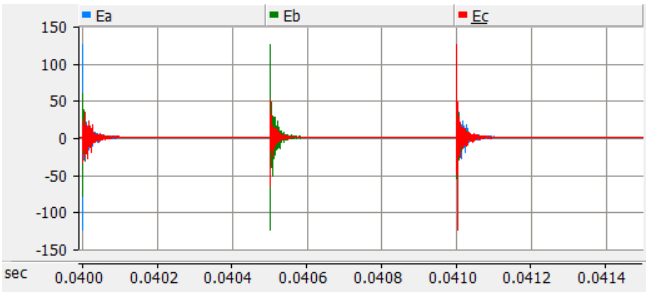

FIGURE 23. **Snapshot of pre-fault reference pulse response.**

Finally, from the 200 simulation runs snapshots are created with a slightly longer time interval (2.01 ms), as the fault event itself is also included. One example (Node 1, Fault R-ground and R_fault = 0.01 Ω is shown in Fig. 24.

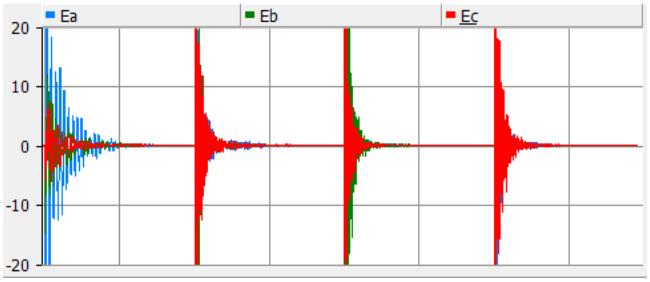

FIGURE 24. Example of pulses responses after a fault event (x: 250 µs/div, y: 10 V/div). Snapshot of pre-fault reference pulse response.

Each snapshot was saved in csv text format and all snapshots together formed the basis for crating the database of fault signals.

IX. RESULTS

In this section, we explain how we are going to structure the experiments.

First, a study of real signal injected in a line without bifurcations.

Second, we perform a study of pulse injection response in a modelled line without bifurcation

Thirdly, we conduct a comparative study similar to the previous one, but with a bifurcation. The idea here is to see how the signal changes with a bifurcation.

In fourth place, a study of impedance influence on the response to the injected pulse.

In fifth place, we make a comparison of responses of the line to a different pulse width.

lastly, we make a comparison between the response signals of the complete modeled real network and the signals obtained in the pilot experience installed on the real line. The objective here is to determine the degree of validity of the signals obtained in the simulation with respect to the real ones.

A. Study of real signals injected in a simple section without bifurcations.

In this experiment, we are going to demonstrate that the theory of the telegrapher's equation presented in Chapter IV THEORY, on which our work is based, is true in reality. To do this, we have made several tests injecting pulses in a simple line formed by a coaxial cable linking the signal injector with the oscilloscope.

The injector has an output impedance of 50 Ω, while the oscilloscope has an input impedance of 1 MΩ.

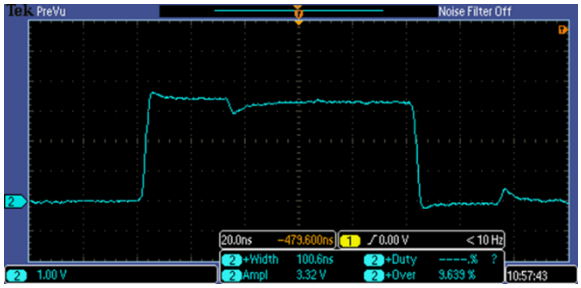

FIGURE 25. Injection pulse width = 100 ns

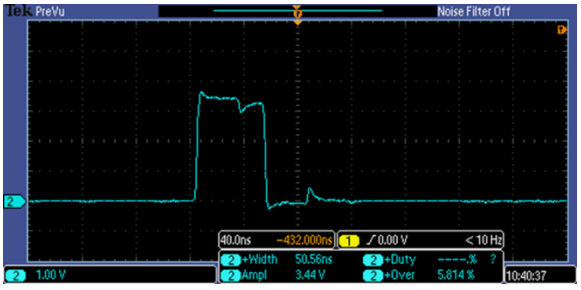

FIGURE 26. Injection pulse width = 30 ns

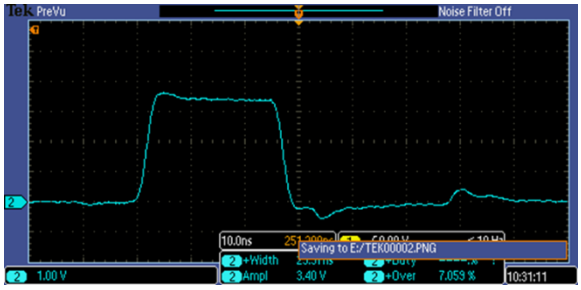

FIGURE 27. Injection pulse width = 50 ns

According to the theory, as there is an impedance mismatch between the injector and the impedance of the oscilloscope, (which here plays the role of an open line end with ∞ impedance), part of the injected signal must bounce back and return to the injector.

In Fig. 25 and Fig. 26 shows how, after injection of a positive signal edge, a signal appears after about 40 ns.

This signal is of opposite sign to the injected signal and of much lower amplitude. The time in which it appears is in accordance with the distance of the cable between the injector and the oscilloscope.

It is also observed that there is a signal bounce for each edge. One bounce as a consequence of the injection of the

positive edge of the signal, and another as a consequence of the negative edge. Both signal bounces have opposite polarity to the signal that generated them.

In Fig. 27 even shows that, if the pulse width is sufficiently small, the two bounces appear once the pulse has finished and each bounces appears approximately 35 ns from the signal that originated it. This reflection time changes according to the distance of the cable used.

In our case for a cable length of 2.5 m and taking into account that the propagation speed of electric current in such a cable is 0.66 c and that the pulse has to travel three times the length of the cable (pulse going to the oscilloscope, bouncing to the injector and bouncing to the oscilloscope again) to be "seen" by the oscilloscope. According to (2) the length of the cable would be:

$$cable\ length = \frac{35ns\ (time\ travel\ pulse) \times \left(300\frac{m}{\mu s}\right).0.6(speed\ of\ signal)}{(1000ns) \times 3\ (number\ of\ trips)} \approx 2.5\ m \quad (19)$$

B. *Study of simulated signals in a simple section without bifurcations.*

In this experiment, we try to reproduce the pulse bounce phenomenon to check if our simulation is correct.

FIGURE 28. Simulation of simple line 300m long

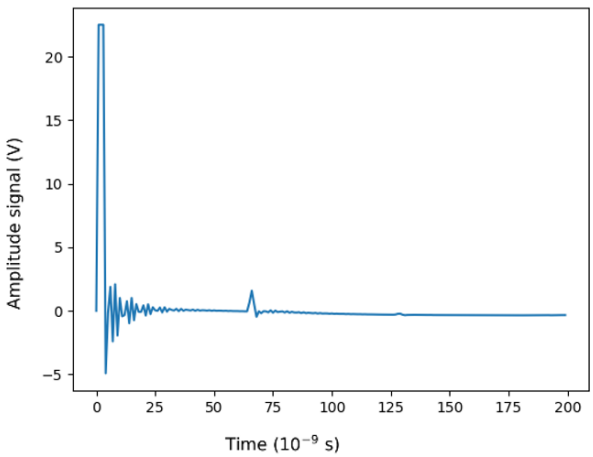

FIGURE 29. Line response to a pulse

Fig. 29 shows how in the simulation, we have injected a pulse of 5 ns width and 24v amplitude.
After about 63 ns the pulse bounce appears at the end of the line.

According to (3), the distance to the end of the line is:

$$cable\ length = \frac{63 \times 50ns \cdot 10^5 \times \left(300\frac{m}{\mu s}\right) \times 0.6}{2} = 297\ m \quad (20)$$

which is consistent with the length of the simulated line

C. *Study of simulated signals in a section with bifurcation.*

This section shows (Fig. 31) the response of a bifurcated network (Fig. 30).

A fault has occurred on this line at 1100 m. The upper part of the figure shows the response of the network without fault, in which it is possible to distinguish perfectly the rebound generated at the bifurcation and the one coming from the end of the line. The lower half of the figure shows the presence of a rebound of negative sign, which starts around 1100 m, the distance at which the fault occurred.

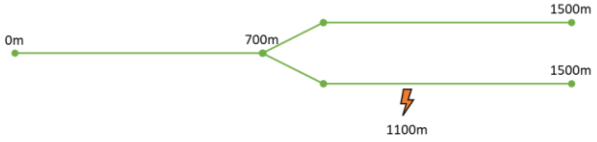

FIGURE 30. Simulation of bifurcation line

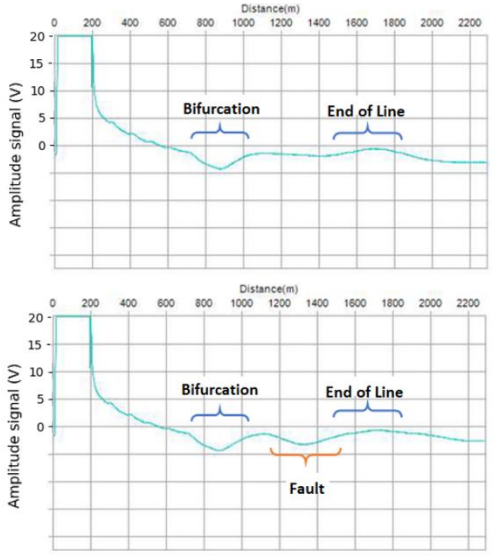

FIGURE 31. Pulse response of bifurcation line

D. Impedance influence on the response to the injected pulse.

Fig. 32 shows the response of a single line without bifurcations to the cases of open-circuit and short-circuit line end.

In the open circuit case, the pulse reaches the end of the line and the bounce generated is of the same sign as the incident signal. On the contrary, in the case where the end of the line is short-circuited, the reflected signal has the opposite sign to the incident signal, and the injector registers a negative pulse. These results confirm the theory of refraction of signals generated in line impedance changes.

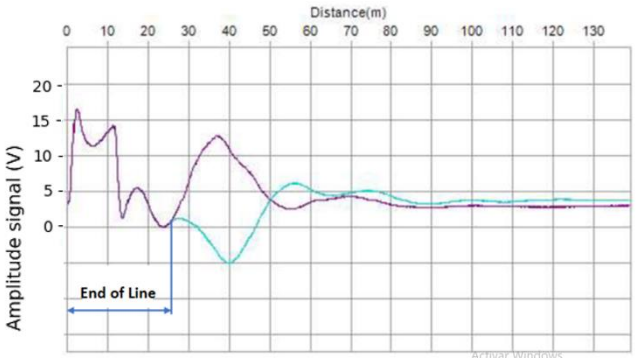

FIGURE 32. Influence of end line impedance value

E. Influence of Pulse Width

As already explained, the proposed localization technique is based on the reflectometry phenomenon and uses the comparison of the network response to a given signal during the pre-fault (PF) and fault (F) states. To evaluate this difference, the "error signal" (E) is defined as the arithmetic difference, sample to sample, between the two signals, both being synchronized at the instant of injection of their respective signals.

For the determination of the pulse width, simulations of low impedance faults have been performed at different locations in the network.

Fig. 33 shows the comparison of 4 simulations employing different pulse widths keeping all other conditions constant. As can be seen in the image, the amplitude of the received signal increases with pulse width, so that a longer time on high of the injected pulse will amplify the received signal, facilitating the measurement of more distant faults.

This amplification occurs up to a certain point, since if the pulse width is increased too much its characteristic frequency will approach the cutoff frequency of the network filter and will be attenuated by it. In this case it has been detected that the maximum received amplitude occurs for a pulse width of 2 µs (Fig. 33 (c)).

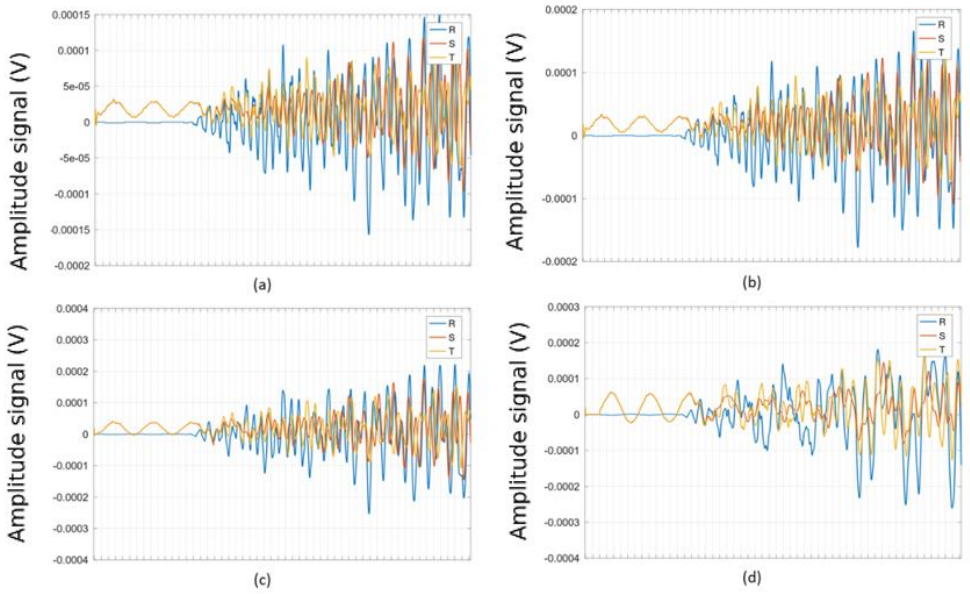

FIGURE 33. Error signal in phases R, S and T, for a low impedance fault located at a distance of 594 m in the network model for a pulse width of: (a) 0.5 µs, (b) 1 µs, (c) 2 µs, (d) 10 µs.

F. Comparative study between the simulated signals and those obtained in the field installation.

This section shows a comparison between the response to an injected pulse in the modeled network and the real network (Fig.34 and Fig.35) where the prototype injector has been installed.

The injector is placed at the same point in the network. It can be seen that the signals have a similar appearance in the time domain.

In the frequency domain it can be observed that the real signal contains a spectrum richer in frequencies. The simulation is a good approximation to the real network.

Even so, the discrepancies between the two signals are to be expected since the modeled network is in a given state with the impedances (loads) in that state during the pulse injection.

In the real network response, the network is in general, in a different state from that of the simulation.

For this reason, in this TDR technique, pulses are constantly injected in the pre-fault state. Thus, the "picture" of the current state of the network is obtained.

When the fault occurs, a pulse is injected again, and that response is processed together with the pre-fault one.

In both cases, the state of the network is the same and, in the variations, will be the information of the type and the distance to the fault. This information can be extracted by appropriate algorithms.

Fig. 36 shows the actual field-assembled prototype with which the real signals have been injected.

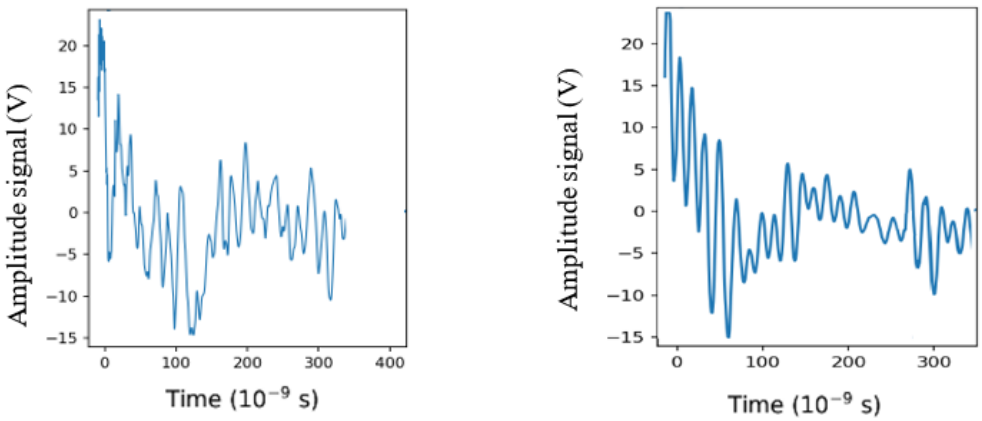

FIGURE 34. Time domain network response to an injected pulse (left) real and (right) modelled

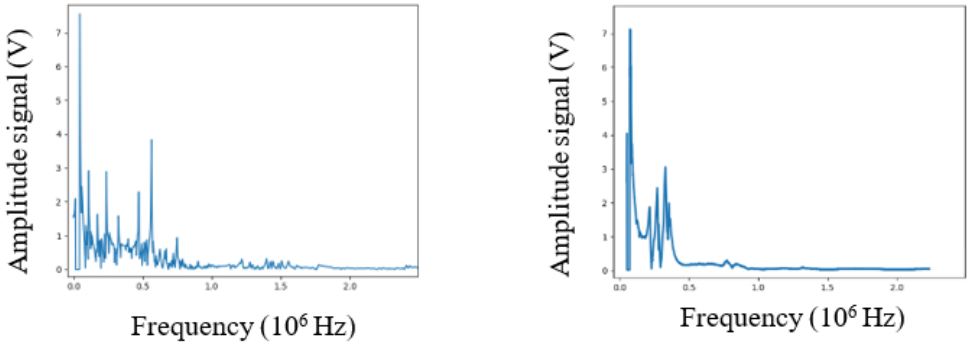

FIGURE 35. FFT network response to an injected pulse (left) real and (right) modelled

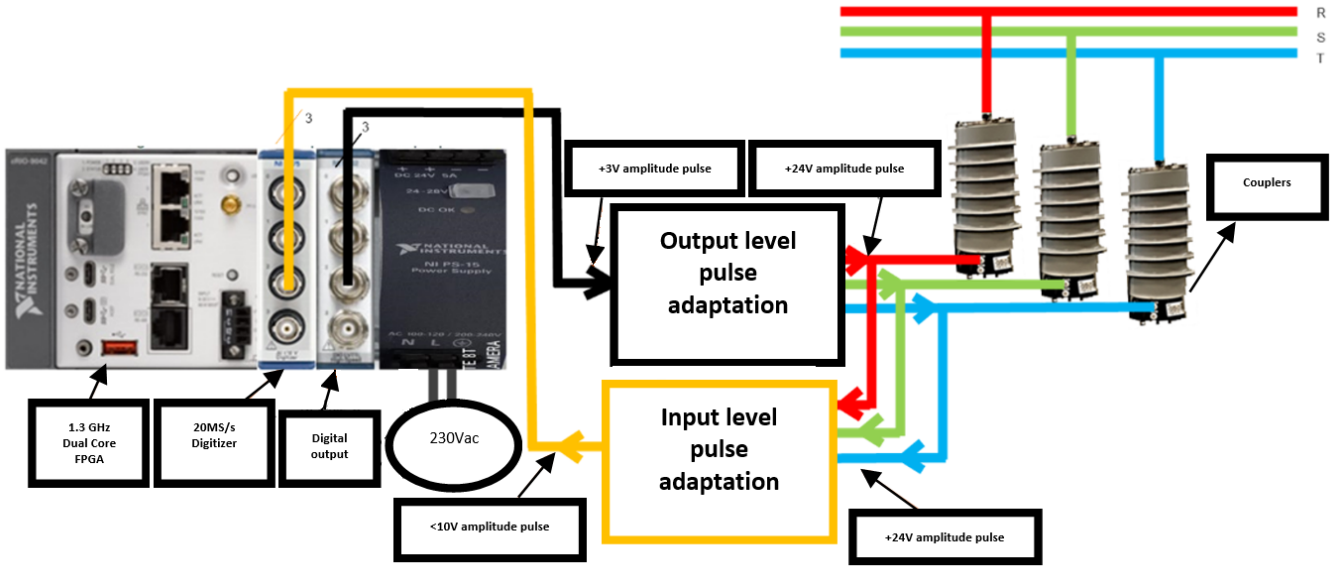

FIGURE 36. Real prototype installed

This prototype is a work of the CIRCE research group and will be presented at a congress that is in the process of being developed.

X. CONCLUSION

TDR technology has been developed during the last years in the research center linked to this work.

Through different European projects we have been advancing in the research in this field.

In the first place, we have reached news milestones in the TDR technique:

- Modeling a real complex network, simulating and obtaining response signals from this network.
- Verify the validity of these signals by comparing them with those of real equipment developed and installed in the field.
- Additionally, these signals (which are also provided in this work as additional material) have been used as a database in another published work [[37]]. In this work a method has been developed to augment the initial database and a Siamese network has been trained to detect and classify faults as a preliminary step to localization.

XI. Future work

Our future short-term points of interest are as follows:
1. To explore and improve the limit of the TDR technique in terms of the largest value detectable/locatable fault impedance value.
2. To explore whether the TDR method is affected by the presence of distributed generations in distribution networks.
3. To explore the possibility of extracting more complex information, such as aging of cables, splices, etc.
5. Finally, we believe that this TDR technique has a huge potential to be continued, investigating in larger ranges, injection frequencies, multi-point injections, etc.

REFERENCES

[1] L. Peretto, R. Tinarelli, A. Bauer, and S. Pugliese, "Fault location in underground power networks: A case study," ISGT 2011. pp. 1–6, 2011. doi: 10.1109/ISGT.2011.5759198.
[2] A. Bahmanyar, S. Jamali, A. Estebsari, and E. Bompard, "A comparison framework for distribution system outage and fault location methods," Electric Power Systems Research, vol. 145, pp. 19–34, Apr. 2017, doi: 10.1016/j.epsr.2016.12.018.
[3] J. H. Teng, W. H. Huang, and S. W. Luan, "Automatic and Fast Faulted Line-Section Location Method for Distribution Systems Based on Fault Indicators," IEEE Transactions on Power Systems, vol. 29, no. 4. pp. 1653–1662, 2014. doi: 10.1109/TPWRS.2013.2294338.
[4] M. Abad López, "Algoritmos de localización de faltas en redes eléctricas," Zaragoza, 2016.
[5] S. Robson, A. Haddad, and H. Griffiths, "Fault Location on Branched Networks Using a Multiended Approach," IEEE Transactions on Power Delivery, vol. 29, no. 4. pp. 1955–1963, 2014. doi: 10.1109/TPWRD.2014.2302137.
[6] K. Sun, Q. Chen, and Z. Gao, "An Automatic Faulted Line Section Location Method for Electric Power Distribution Systems Based on Multisource Information," IEEE Transactions on Power Delivery, vol. 31, no. 4. pp. 1542–1551, 2016. doi: 10.1109/TPWRD.2015.2473681.
[7] S. Lotfifard, M. Kezunovic, and M. J. Mousavi, "A Systematic Approach for Ranking Distribution Systems Fault Location Algorithms and Eliminating False Estimates," IEEE Transactions on Power Delivery, vol. 28, no. 1. pp. 285–293, 2013. doi: 10.1109/TPWRD.2012.2213616.
[8] R. J. Hamidi and H. Livani, "Traveling-Wave-Based Fault-Location Algorithm for Hybrid Multiterminal Circuits," IEEE Transactions on Power Delivery, vol. 32, no. 1. pp. 135–144, 2017. doi: 10.1109/TPWRD.2016.2589265.
[9] A. Farughian, L. Kumpulainen, and K. Kauhaniemi, "Review of methodologies for earth fault indication and location in compensated and unearthed MV distribution networks," Electric Power Systems Research, vol. 154, no. Supplement C, pp. 373–380, 2018, doi: https://doi.org/10.1016/j.epsr.2017.09.006.
[10] P. Stefanidou-Voziki, N. Sapountzoglou, B. Raison, and J. L. Dominguez-Garcia, "A review of fault location and classification methods in distribution grids," Electric Power Systems Research, vol. 209, no. May, 2022, doi: 10.1016/j.epsr.2022.108031.
[11] S. S. Gururajapathy, H. Mokhlis, and H. A. Illias, "Fault location and detection techniques in power distribution systems with distributed generation: A review," Renewable and Sustainable Energy Reviews, vol. 74, pp. 949–958, Jul. 2017, doi: 10.1016/j.rser.2017.03.021.
[12] Y. Q. Chen, O. Fink, and G. Sansavini, "Combined Fault Location and Classification for Power Transmission Lines Fault Diagnosis With Integrated Feature Extraction," IEEE Transactions on Industrial Electronics, vol. 65, no. 1, pp. 561–569, 2018, doi: 10.1109/TIE.2017.2721922.
[13] H. Ungrad, W. Winkler, and A. Wiszniewski, "Protection Techniques in Electrical Energy Systems," Protection Techniques in Electrical Energy Systems, Aug. 2020, doi: 10.1201/9781003067504/PROTECTION-TECHNIQUES-ELECTRICAL-ENERGY-SYSTEMS-HELMUT-UNGRAD-WILLIBALD-WINKLER-ANDRZEJ-WISZNIEWSKI.
[14] J. Oasa et al., " 'Verification of fault location by TDR measurement on an actual line including multiple ground-mounted equipment,' 2021.".
[15] R. Lacoste, "'Time Domain Reflectometry,' Robert Lacoste's The Darker Side, pp. 33–47, 2010, doi: 10.1016/B978-1-85617-762-7.00003-4.".
[16] R. Dashti, S. M. Salehizadeh, H. R. Shaker, and M. Tahavori, "Fault location in double circuit medium power distribution networks using an impedance-based method," Applied Sciences (Switzerland), vol. 8, no. 7, 2018, doi: 10.3390/app8071034.
[17] M. Shafiullah and M. A. Abido, "S-Transform Based FFNN Approach for Distribution Grids Fault Detection and Classification," IEEE Access, vol. 6, 2018, doi: 10.1109/ACCESS.2018.2809045.
[18] A. Aljohani, A. Aljurbua, M. Shafiullah, and M. A. Abido, "Smart fault detection and classification for distribution grid hybridizing ST and MLP-NN," in 2018 15th International Multi-Conference on Systems, Signals and Devices, SSD 2018, 2018. doi: 10.1109/SSD.2018.8570582.
[19] A. Ekka and A. Yadav, "Fault Identification Using Fuzzy In Renewable Energy Interfaced IEEE 13 Bus System; Fault Identification Using Fuzzy In Renewable Energy Interfaced IEEE 13 Bus System," 2022, doi: 10.1109/ICICCSP53532.2022.9862498.
[20] F. J. L. Padua and R. de Oliveira, "Allocation of PLC Devices in a Low-Voltage Grid," 2019 IEEE PES Conference on Innovative Smart Grid Technologies, ISGT Latin America 2019, Sep. 2019, doi: 10.1109/ISGT-LA.2019.8895457.
[21] M. P. Sibanda, P. A. Janse Van Rensburg, and H. C. Ferreira, "Impedance matching with low-cost, passive components for narrowband PLC," 2011 IEEE International Symposium on Power Line Communications and Its Applications, ISPLC 2011, pp. 335–340, 2011, doi: 10.1109/ISPLC.2011.5764418.
[22] M. P. Sibanda, P. A. J. van Rensburg, and H. C. Ferreira, "A compact economical PLC band-pass coupler with impedance matching," ISPLC 2013 - 2013 IEEE 17th International Symposium on Power Line Communications and Its Applications, Proceedings, no. 1, pp. 339–344, 2013, doi: 10.1109/ISPLC.2013.6525874.
[23] J. Mora-Flòrez, J. Meléndez, and G. Carrillo-Caicedo, "Comparison of impedance based fault location methods for power distribution systems," Electric Power Systems Research, vol. 78, no. 4, pp. 657–666, 2008, doi: https://doi.org/10.1016/j.epsr.2007.05.010.
[24] A. Farughian, L. Kumpulainen, and K. Kauhaniemi, "Review of methodologies for earth fault indication and location in compensated and unearthed MV distribution networks," Electric Power Systems Research, vol. 154, no. Supplement C, pp. 373–380, 2018, doi: https://doi.org/10.1016/j.epsr.2017.09.006.
[25] C. Galvez and A. Abur, "Fault Location in Active Distribution Networks Containing Distributed Energy Resources (DERs)," IEEE Transactions on Power Delivery, vol. 36, no. 5, pp. 3128–3139, 2021, doi: 10.1109/TPWRD.2020.3034179.
[26] H. Mirshekali, R. Dashti, A. Keshavarz, A. J. Torabi, H. R. Shaker, and S. Member, "A Novel Fault Location Methodology for Smart Distribution Networks," vol. 12, no. 2, pp. 1277–1288, 2021, doi: 10.1109/TSG.2020.3031400.
[27] X. Lin, F. Zhao, G. Wu, Z. Li, and H. Weng, "Universal Wavefront Positioning Correction Method on Traveling-Wave-Based Fault-Location Algorithms," IEEE Transactions on Power Delivery, vol. 27, no. 3, pp. 1601–1610, 2012, doi: 10.1109/TPWRD.2012.2190108.
[28] L. Peretto, R. Tinarelli, A. Bauer, and S. Pugliese, "Fault location in underground power networks: A case study," ISGT 2011. pp. 1–6, 2011. doi: 10.1109/ISGT.2011.5759198.

[29] R. J. Hamidi and H. Livani, "Traveling-Wave-Based Fault-Location Algorithm for Hybrid Multiterminal Circuits," IEEE Transactions on Power Delivery, vol. 32, no. 1. pp. 135–144, 2017. doi: 10.1109/TPWRD.2016.2589265.
[30] C. Zhou, Q. Shu, X. Han, and C. Qin Shu, "A single-phase earth fault location scheme for distribution feeder on the basis of the difference of zero mode traveling waves," no. August 2016, pp. 1–9, 2017, doi: 10.1002/etep.2298.
[31] W. Chonglin, W. Yangyang, L. Rui, and S. Gang, "Fault Location for Single-Phase-To-Earth Faults Based on Transient Traveling Wave Method and Artificial Pulse Signal Injection Method," in 2010 International Conference on Electrical and Control Engineering, 2010, pp. 3737–3741. doi: 10.1109/iCECE.2010.912.
[32] M. Abad, S. Borroy, D. López, and M. García-gracia, "New Fault Location Method for up-to-date and Upcoming Distribution Networks," CIRED 23 rd International Conference on Electricity Distribution, no. 1290, 2015.
[33] J. Livie, P. Gale, and A. Wang, "Experience With On-Line Low Voltage Cable Fault Location Techniques in Scottish Power," CIRED 19th International Conference on Electricity Distribution, no. 0696, 2007.
[34] S. S. Gururajapathy, H. Mokhlis, and H. A. Illias, "Fault location and detection techniques in power distribution systems with distributed generation: A review," Renewable and Sustainable Energy Reviews, vol. 74, pp. 949–958, Jul. 2017, doi: 10.1016/j.rser.2017.03.021.
[35] M. A. Aftab, S. M. S. Hussain, I. Ali, and T. S. Ustun, "Dynamic protection of power systems with high penetration of renewables: A review of the traveling wave based fault location techniques," International Journal of Electrical Power and Energy Systems, vol. 114, no. May 2019, p. 105410, 2020, doi: 10.1016/j.ijepes.2019.105410.
[36] A. Bahmanyar, S. Jamali, A. Estebsari, and E. Bompard, "A comparison framework for distribution system outage and fault location methods," Electric Power Systems Research, vol. 145, pp. 19–34, 2017, doi: 10.1016/j.epsr.2016.12.018.
[37] J. G. Fornas, E. H. Jaraba, A. L. Estopinan, and J. Saldana, "Detection and Classification of Fault Types in Distribution Lines by Applying Contrastive Learning to GAN Encoded Time-series of Pulse Reflectometry Signals.," IEEE Access, pp. 1–1, 2022, doi: 10.1109/ACCESS.2022.3214994.

JAVIER GRANADO FORNÁS received the B.Sc. in industrial engineering (specialized in industrial electronics) and M.Sc. degrees in electronics engineering (intelligent environments specialization) from the University of Zaragoza, Spain, in 1994 and 2014, respectively. He is currently pursuing the Ph.D. degree in Deep Learning around classification and localization of faults in distributions lines. Since 2009, he has been working as a Senior Researcher with the Electronics Systems Group at CIRCE Technology Center. His main research interests include electronic designs control projects around Deep Learning and algorithms for fault detection.

ELÍAS HERRERO JARABA has a PhD in Engineering from the University of Zaragoza since June 2005, and has been a professor at the University of Zaragoza since 2002. In 1999, and for 4 years, he worked in the automotive field at Opel Spain, in the production department.
Within the university he has developed his research in the area of computer vision, and since 2012 he has focused his interest in the field of neural networks, and more recently, in Deep Learning. In the meantime, he held the position of coordinator of the Smart Vehicle initiative of the Aragon Institute for Engineering Research (I3A).
He currently holds a European patent and has led to more than six projects funded in public competitions, more than 20 projects with companies, 12 indexed publications, and more than 50 contributions to international conferences.
It is worth mentioning the 3M award for his research in the CvLAB research group.
His teaching work has focused on electronics, from its basics to power electronics, including embedded systems.

HANS BLUDSZUWEIT PhD in electrical engineering. Born in Jena (Germany) in 1974, received the Dipl.-Ing. degree in Electrical Engineering from the Technical University of Ilmenau (Germany) in 2001 and the PhD (European Doctorate) from the University of Zaragoza (Spain) in 2009. Since 2009 he is a researcher in the Electrical Systems Area at CIRCE, where he is currently Technological Expert in the Smart Grid Operation Group. His activity is focused on Smart Grids (optimization of distributed resources, including storage and statistical analysis of Smart Meter data) and grid integration of electric vehicles, including dynamic wireless charging (e-roads). He worked one year as field test engineer in the sector of solar PV module production among others in the company First Solar.

DAVID CERVERO GARCÍA received the B.Sc. degree in industrial engineering (specialized in electric systems), and the M.Sc. degree in Renewable Energies and Energy Efficiency from the University of Zaragoza in 2009 and 2011, respectively. Currently, he is working as Project Manager in the Electronic Systems group at CIRCE Technology Centre.
He has a deep expertise in power quality (PQ) assessment in electrical systems, data acquisition and, specially, in digital signal processing, developing dedicated software for

measuring PQ in electrical distribution networks and performance of renewable energy sources. Fault location and power systems monitoring, with application in predictive maintenance, are among his research fields of interest. Currently, his main research field is focused on designing resonant converters for high voltage applications.

ANDRÉS LLOMBART ESTOPIÑAN is the General Director of CIRCE since April 2016 and former Executive Director since January 2011. He was also a lecturer of the Electrical Department at University of Zaragoza since June 2003 to May 2018. In November 2011 was designated by the Science and innovation Ministry as the expert in Energy Area Committee of the7th Funding Program of the European Union, being in charge of the coordination of electricity grids topics. In CIRCE, he is in charge of Innovation and Promotion Unit, created by himself on May 2009.
From March 2007 until March 2009, he was Subdirector of Institutional Relations of the Superior Polytechnic Centre of the University of Zaragoza.
In 1994, he received an Industrial Engineer degree at the University of Zaragoza. Later, he researched the impact reduction of power electronic source grids using passive filters in the kilowatt range. This research gave him a PhD title (specialised in electrical engineering) by the University of Zaragoza in 2000. From December 1994 to May 2001, he was an associate professor in the Electrical Engineering Department at the University of Zaragoza, where he performed the following teaching activities: electric circuit theory,